**Proposal to Jefferson Lab PAC 39**

# C-REX: PARITY-VIOLATING MEASUREMENT of the WEAK CHARGE DISTRIBUTION of $^{48}$Ca to 0.03 fm ACCURACY


Spokespersons: J. Mammei, R. Michaels, K. Paschke, S. Riordan*, P.A.Souder

J. Mammei, S. Riordan, K. Kumar, J. Wexler
*University of Massachusetts, Amherst*

K. Paschke, G.D. Cates, M. Dalton, X. Zheng
*University of Virginia*

P.A. Souder, R. Holmes, L. Zana
*Syracuse University*

R. Michaels, K. Allada, A. Camsonne, J. Benesch, J.P. Chen, D. Gaskell
O. Hansen, D.W. Higinbotham, J. Gomez, J. LeRose, B. Moffit, S. Nanda,
B. Wojtsekhowski, J. Zhang
*Thomas Jefferson National Accelerator Facility*

Konrad Aniol
*California State University, Los Angeles*

G.B. Franklin, B. Quinn
*Carnegie Mellon Univerisity*

P. Markowitz
*Florida International University*

*) contact spokesperson, riordan@jlab.org

E. Cisbani, A. del Dotto, S. Frullani, F. Garibaldi
*INFN Roma gruppo collegato Sanità*
*and Italian National Institute of Health, Rome, Italy*

M. Capogni
*INFN Roma gruppo collegato Sanità*
*and ENEA Casaccia, Rome, Italy*

V. Bellini, A. Giusa, F. Mammoliti, G. Russo, M.L. Sperduto, C.M. Sutera
*INFN - Sezione di Catania*

D. McNulty
*Idaho State University*

C.J. Horowitz
*Indiana University*

M. Mihovilovič, S. Širca
*Jožef Stefan Institute and University of Ljubljana, Slovenia*

A. Glamazdin
*Kharkov Institute of Physics and Technology*

T. Holmstrom
*Longwood University*

R. Mahurin
*University of Manitoba*

S. Kowalski, V. Sulkosky
*Massachusetts Institute of Technology*

S.K. Phillips
*University of New Hampshire*

P. King, J. Roche
*Ohio University*

F. Meddi, G.M. Urciuoli
*Sapienza University of Rome and INFN - Sezione di Roma*

A. Blomberg, Z.-E. Meziani, N. Sparveris
*Temple University*

M. Pitt
*Viriginia Polytechnic Institute and State University*

D. Armstrong, J.C. Cornejo, W. Deconinck, J.F. Dowd, V. Gray, and J. Magee
*College of William and Mary*

D. Androic
*University of Zagreb*

**A Hall A Collaboration Proposal**

The proposal and related information is at
http://hallaweb.jlab.org/parity/prex

## ABSTRACT

We propose to measure the parity-violating asymmetry for elastic scattering from $^{48}$Ca at E = 2.2 GeV and $\theta = 4^{\circ}$. This will provide a measurement of the weak charge distribution and hence the neutron density at one value of $Q^2 = 0.022$ GeV$^2/c^2$. It will provide an accuracy in the neutron radius $R_n$ equivalent to $\pm 0.03$ fm ($\sim 0.9\%$). A measurement this precise will have a significant impact on nuclear theory, particularly on the topic of 3-neutron forces. Further, together with the planned $R_n^{208}$ measurement, $R_n^{48}$ will provide vital input in many areas such as neutron star structure, heavy ion collisions and atomic parity violation. A precise measurement on a small nucleus is favorable because it can be measured at high momentum transfer where the asymmetry is larger (for the proposed kinematics, about 2 ppm). Also, since $^{48}$Ca is neutron-rich it has a larger weak charge and greater sensitivity to $R_n$. We are requesting 40 days of polarized beam running in Hall A at a 1-pass energy of 2.2 GeV using a septum magnet to reach a $4^{\circ}$ scattering angle. The experimental setup is similar to PREX. This beam time request includes 30 days of production data-taking and 5 days of commissioning and 5 days of overhead for Møller polarimetry and other auxiliary measurements.

# C-REX : $^{48}$Ca Parity

## I SCIENTIFIC MOTIVATION

We propose to measure the parity-violating longitudinal single-spin asymmetry for elastic scattering from $^{48}$Ca, which will serve as an important complement to a similar measurement using $^{208}$Pb. In combination, the results will challenge the assumptions of state-of-the-art nuclear structure models, with measurements for atomic mass number $A$ in a regime where microscopic models can be applied to a regime in which the nucleon closely approximates infinite neutron-rich nuclear matter. By itself, $^{48}$Ca can help illuminate specific details such as the role of three-neutron forces in these microscopic calculations.

Viewed from another perspective, under the assumptions of present nuclear theory the two measurements are expected to be strongly correlated, so a precise result on $^{48}$Ca would reinforce the precision of the PREX measurement on $^{208}$Pb. This provides a route to significantly improve the precision of an important constraint on the symmetry energy density dependence. This route allows us to overcome the limitations in performing the measurements as the uncertanties in both are mostly uncorrelated.

The determination of the density of the distribution of neutrons in complex nuclei through measurements of the parity-violating asymmetry is explained in Sec. I A. We describe the broad implications of these measurements in section Sec. I B, the present status of experiments in Sec. I C, and detail the specific role of the proposed measurement of the neutron radius of $^{48}$Ca in Sec. I D. In addition, the motivation for a short extension of this proposal to measure the parity-conserving transverse single-spin asymmetry $A_T$ from $^{48}$Ca is described in Sec.I E.

### A Parity Violating Measurements of Neutron Densities

The charge density $\rho_{ch}$ of heavy nuclei can be obtained by taking the Fourier transform of $F_{ch}(Q^2)$, the form factor for elastic electron scattering. Indeed, an extensive set of measurements covering a large range of $Q^2$ and many isotopes

has provided a detailed picture of the shapes of nuclei [1]. Since the electron interacts through the well-known electromagnetic interaction, the interpretation of these results are theoretically clean. In contrast, our knowledge of neutron densities comes primarily from hadron scattering experiments involving, for example, pions [2], protons [3–5], antiprotons [6,7] or alpha particles [8,9], the interpretation of which requires a model-dependent description of the non-perturbative strong interaction. An alternative approach is to exploit the fact that the $Z$-boson couples much more strongly to neutrons than protons, so parity-violation in elastic electron scattering is sensitive to the neutron density distribution $\rho_n$. Again, since the probe is electroweak, the measurement of parity-violation in electron scattering provides a model-independent probe of neutron densities that is free from most strong-interaction uncertainties [10].

In the Born approximation, the parity-violating asymmetry of the cross section for longitudinally polarized electrons elastically scattered from an unpolarized nucleus, $A_{PV}$, is proportional to the weak form factor $F_W(Q^2)$. This is the Fourier transform of the weak charge density, which is closely related to the neutron density, and therefore the neutron density can be extracted from an electro-weak measurement [10]. In the limit $Q^2 \ll M_Z^2$, this asymmetry is given by

$$A_{PV} = \frac{\sigma_R - \sigma_L}{\sigma_R + \sigma_L} \approx \frac{G_F Q^2}{4\pi\alpha\sqrt{2}} \frac{F_W(Q^2)}{F_{ch}(Q^2)}, \tag{1}$$

where $\sigma_{R(L)}$ is the differential cross section for elastic scattering of right- (R) and left- (L) handed longitudinally polarized electrons, $G_F$ is the Fermi constant, $\alpha$ the fine structure constant, and $F_{ch}(Q^2)$ is the Fourier transform of the known charge density. For a heavy nucleus Coulomb-distortion effects are large and must be included. These have been accurately calculated [11] exploiting the fact that the charge density is well known. Many other details relevant for a practical parity-violation experiment to measure neutron densities have been discussed in a previous publication [12].

## B Importance of $R_n$ in Nuclear Physics and Astrophysics

The size of the neutron radius $R_n$ in neutron-rich nuclei has important implications for models of nuclear structure and their application in atomic physics and astrophysics. For neutron-rich heavy nuclei, some of the excess neutrons is expected to be found in the surface, where they form a neutron-rich skin. The thickness of this skin, that is, the difference between the neutron and pro-

ton radius $R_n - R_p$, is sensitive to nuclear dynamics and provides fundamental nuclear structure information.

This insight motivated the PREX and PREX-II experiments on $^{208}$Pb. The large, doubly-magic $^{208}$Pb nucleus, with 44 more neutrons than protons, was identified as an excellent laboratory for the study of the neutron skin in heavy nuclei. There is a strong correlation between the neutron radius in $^{208}$Pb, $R_n^{208}$, and the pressure of neutron matter $P$ at densities near 0.1 fm$^{-3}$ (about 2/3 of nuclear density) [13]. A larger $P$ will push neutrons out against surface tension and increase $R_n$. Therefore measuring $R_n^{208}$ constrains the equation-of-state (EOS), the pressure as a function of density, of neutron matter.

To illuminate the importance of the measurement of $R_n$ in nuclear matter, we review some of the implications of the proposed PREX-II measurement of neutron radius in $^{208}$Pb. The relationship with the proposed measurement of $R_n$ for the relatively light $^{48}$Ca nucleus will be detailed in Sec. I D.

The correlation between $R_n^{208}$ and the radius of a neutron star, $r_{NS}$, is very interesting [14]. In general, a larger $R_n$ implies a stiffer EOS , with a larger pressure, that correlates to larger $r_{NS}$. Recently there has been great progress in deducing $r_{NS}$ from X-ray observations. The value of $r_{NS}$ is deduced from the spectrum and intensity of the X-rays, with model-dependent corrections for the properties of the atmosphere of the neutron star. The state of the art is as follows. From observations of X-ray bursts from three-ideal neutron stars, Ozel *et al.* [15] find $r_{NS}$ is very small, near 10 km, implying that the EOS softens at high density which is suggestive of a transition to an exotic phase of QCD. In contrast, Steiner *et al.* [16], using the same three neutron stars plus six more, conclude that $r_{NS}$ is near 12 km, leading to a prediction that $R_n^{208} - R_p^{208} = 0.15 \pm 0.02$ fm. This implies a stiffer EOS which leaves little room for softening due to a phase transition at high density.

The EOS of neutron-rich matter is closely related to the symmetry energy $S$. There is an empirical strong correlation between $R_n^{208}$ and the density dependence of the symmetry energy $dS/d\rho$, with $\rho$ as the baryon density. The density dependence of the symmetry energy can be probed in heavy-ion collisions [17]. For example, $dS/d\rho$ has been extracted from isospin diffusion data [18] using a transport model.

The symmetry energy $S$ is an important parameter when evaluating the composition and structure of a neutron star. A large $S$ at high density would imply a large proton fraction, which would allow the direct Urca process [19] of rapid neutrino cooling. If $R_n^{208} - R_p^{208}$ were large, it is likely that massive neutron stars would cool quickly by direct Urca. In addition, the transition density from a solid neutron star crust to the liquid interior is strongly correlated with $R_n^{208} - R_p^{208}$ [20].

The EOS of neutron stars is also important for the LIGO experiment searching for signals from inspiraling neutron stars. First, the number of neutron stars expected depends upon how fast the stars cool, since only hot neutron

stars may be observed. In addition, the properties of the gravity waves to be observed depends on the EOS [21].

Reinhard and Nazarewicz claim that $R_n^{208} - R_p^{208}$ is tightly correlated with the dipole polarizability $\alpha_D$ [22] and Tamii et al. use this correlation to infer $R_n^{208} - R_p^{208}$ from a new measurement of $\alpha_D$ [23] in $^{208}$Pb. However, Piekarewicz et al. have now shown the correlation of $R_n^{208} - R_p^{208}$ and $\alpha_D$ to be model dependent [28]. This model dependence emphasizes the importance of more model independent electroweak measurements of $R_n$.

In the end, by measuring $A_{PV}$ the experiment unambiguously measures the ratio of neutron to proton form-factors $F_n/F_p$ at a single $Q^2$. With modest model-dependence in the description of the surface thickness in the mean-field description of the nucleus, the neutron radius $R_n$ can be deduced from this measurement. A precise determination of the neutron skin $R_n - R_p$ in $^{208}$Pb provides a constraint on the density dependence of symmetry energy, in a regime where extrapolation to other nuclear species and up to the scale of bulk nuclear matter (*i.e.* neutron star) are possible. However, this extrapolation required model input to describe the variation of the symmetry energy with the size and atomic mass number of the nucleus. This leaves a role for a precision measurement on a smaller nucleus, to benchmark that extrapolation. In addition, under existing models $R_n$ from a light nucleus may be highly correlated to $R_n^{208}$, so such a measurement could be seen as improving the precision of the determination of the density dependence of the symmetry energy.

## C The PREX and PREX-II Experiments on $^{208}$Pb

The PREX experiment measured the parity-violating asymmetry $A_{PV}$ for 1.06 GeV electrons scattered by about five degrees from $^{208}$Pb, with the result [24]

$$A_{PV} = 0.656 \pm 0.060(\text{stat}) \pm 0.014(\text{syst}) \text{ ppm}\,. \tag{2}$$

A major success of PREX was the achievement of the very small systematic error of 0.014 ppm. This strongly suggests that the total error can be significantly improved if more statistics can be obtained.

From Eq. 2, a number of physical quantities were deduced [24], [25]. The form factor $F_W(q)$ of the weak charge density $\rho_W(r)$ for $^{208}$Pb is

$$F_W(q = 0.475 \text{ fm}^{-1}) = \frac{1}{\mathrm{Q_W}} \int \mathrm{d^3 r j_0(qr)} \rho_{\mathrm{W}}(\mathrm{r}) = 0.204 \pm 0.028. \tag{3}$$

Here the total weak charge of $^{208}$Pb is $Q_W$ and $q$ is the momentum transfer of the experiment. The weak radius of $^{208}$Pb (rms radius of $\rho_W(r)$) is

$$R_W = 5.826 \pm 0.181(\text{exp}) \pm 0.027(\text{mod}) \text{ fm}. \tag{4}$$

Here the experimental error includes both statistical and systematic effects while the small model error includes model uncertainties related to the surface thickness. One needs to make very modest assumptions about the surface thickness in order to extract the rms radius from a single measurement at the particular $Q^2$ chosen for the experiment. Comparing Eq. 4 to the well measured (E+M) charge radius $R_{ch} = 5.503$ fm yields a "weak charge skin"

$$R_W - R_{ch} = 0.323 \pm 0.181(\text{exp}) \pm 0.027(\text{mod}) \text{ fm}. \tag{5}$$

Thus the surface region of $^{208}$Pb is relatively enhanced in weak charges compared to electromagnetic charges. This weak charge skin is closely related to the expected neutron skin, as discussed below. Equation 5, itself, represents an experimental milestone. We now have direct evidence that the weak charge density of a heavy nucleus is more extended than the electromagnetic charge density. Finally the neutron skin, difference of the point neutron $R_n^{208}$ and proton $R_p^{208}$ radii of $^{208}$Pb was deduced to be

$$R_n^{208} - R_p^{208} = 0.33^{+0.16}_{-0.18} \text{ fm}. \tag{6}$$

This is a $(1.8\sigma)$ observation of the neutron skin in a heavy nucleus with a purely electroweak reaction.

A second $^{208}$Pb run called PREX-II has now been approved which has a proposed error in $R_n^{208}$ smaller by a factor of three to $\pm 0.06$ fm.

## D Measuring the Neutron Radius of $^{48}$Ca and Three-Nucleon Forces

We now focus on the neutron radius of $^{48}$Ca, $R_n^{48}$. This nucleus has a large neutron excess and is significantly smaller than $^{208}$Pb (3.4 fm vs. 5.8 fm). The smaller size allows $R_n^{48}$ to be measured at a higher $Q^2$ and energy, where the experimental figure-of-merit is larger (discussed in Sec. II E). Thus the experiment has the potential to provide the most sensitive measurement of a neutron skin to date. In the context of existing nuclear models, $R_n^{48}$ is expected to be strongly correlated with $R_n^{208}$ as well as to the density dependence of the symmetry energy (see Appendix A). However, as described below, it is important to note that this correlation depends on the correctness of the existing models, and even in that context the correlation is imperfect. Furthermore, while the larger $^{208}$Pb nucleus is a better approximation of infinite nuclear matter, the structure of $^{48}$Ca can be addressed in detailed, microscopic models that are not presently feasible for $^{208}$Pb. Thus independent electroweak measurements of $R_n^{48}$ and $R_n^{208}$ would provide a test of existing nuclear structure models over a range of $A$, benchmark calculations that attempt to extrapolate descriptions of neutron density of intermediate $A$, and relate the measurement of $R_n$ to

model-dependent description of the underlying dynamics, such as the very interesting subject of three-neutron forces.

Three-nucleon forces are now a vital part of microscopic nuclear structure calculations including Green's function Monte Carlos, no-core shell models, and coupled cluster methods. Often the parameters of three-nucleon forces are fit to reproduce properties of light nuclei. However, there are far fewer constraints on the parameters for three-*neutron* forces. These poorly known forces are very important for very neutron rich systems in astrophysics. It is important to obtain data pertinent to this subject and measuring $R_n^{48}$ should demonstrate the important role of three-neutron forces and constrain their parameters.

Presumably three-nucleon forces are important for $R_n^{208}$, but unfortunately, we do not yet have microscopic calculations for $R_n^{208}$ that can directly show the effects of three-neutron forces. Instead we must rely on the following somewhat indirect procedure. Alex Brown [13] has demonstrated a correlation between $R_n^{208}$ and the pressure of neutron matter at a density of 2/3 of saturation density. Hebeler et al. calculate the effect of three-neutron forces, not in $^{208}$Pb directly, but for the pressure of uniform neutron matter [26]. They find that three-neutron forces, as calculated in chiral effective field theory, significantly increase the pressure of neutron matter compared to calculations that only include two-neutron forces, Fig. 1. Furthermore, the large neutron skin measured by PREX, Eq. 6, is consistent with three-neutron force results, and hints at a larger neutron matter pressure than that predicted by only two-neutron force. Note that this procedure depends crucially on the, possibly somewhat model dependent, correlation between $R_n^{208}$ and the neutron matter pressure.

Measuring $R_n^{48}$ in $^{48}$Ca can remove this model dependence and allow a direct comparison of experimental results to three-neutron force calculations. State of the art Coupled Cluster calculations by Hagen et al. that include three-nucleon forces (as calculated in chiral effective field theory and included as density dependent two body forces) [27] show that three-nucleon forces significantly reduce the binding energy for very neutron rich calcium isotopes and they may change the heaviest particle stable calcium isotope from $^{70}$Ca to $^{60}$Ca. Note this is not yet known experimentally, and there is great interest in studying the properties of very neutron rich calcium isotopes with radioactive beams. There is an important complementarity between precision electroweak measurements on stable systems, such as this proposal, and less precise radioactive beam experiments on even more neutron rich systems.

Hagen et al. are presently working on calculating $R_n^{48}$ for their Coupled Cluster calculations with and without three-nucleon forces. The large change in binding energy and the large increase in the pressure of neutron matter found by Hebeler et al. strongly suggest that three-neutron forces will significantly increase $R_n^{48}$. Note that Hebeler et al. find that three-neutron forces increase $R_n^{208}$ by about 0.05 fm (assuming the correlation with the $P$ of neutron

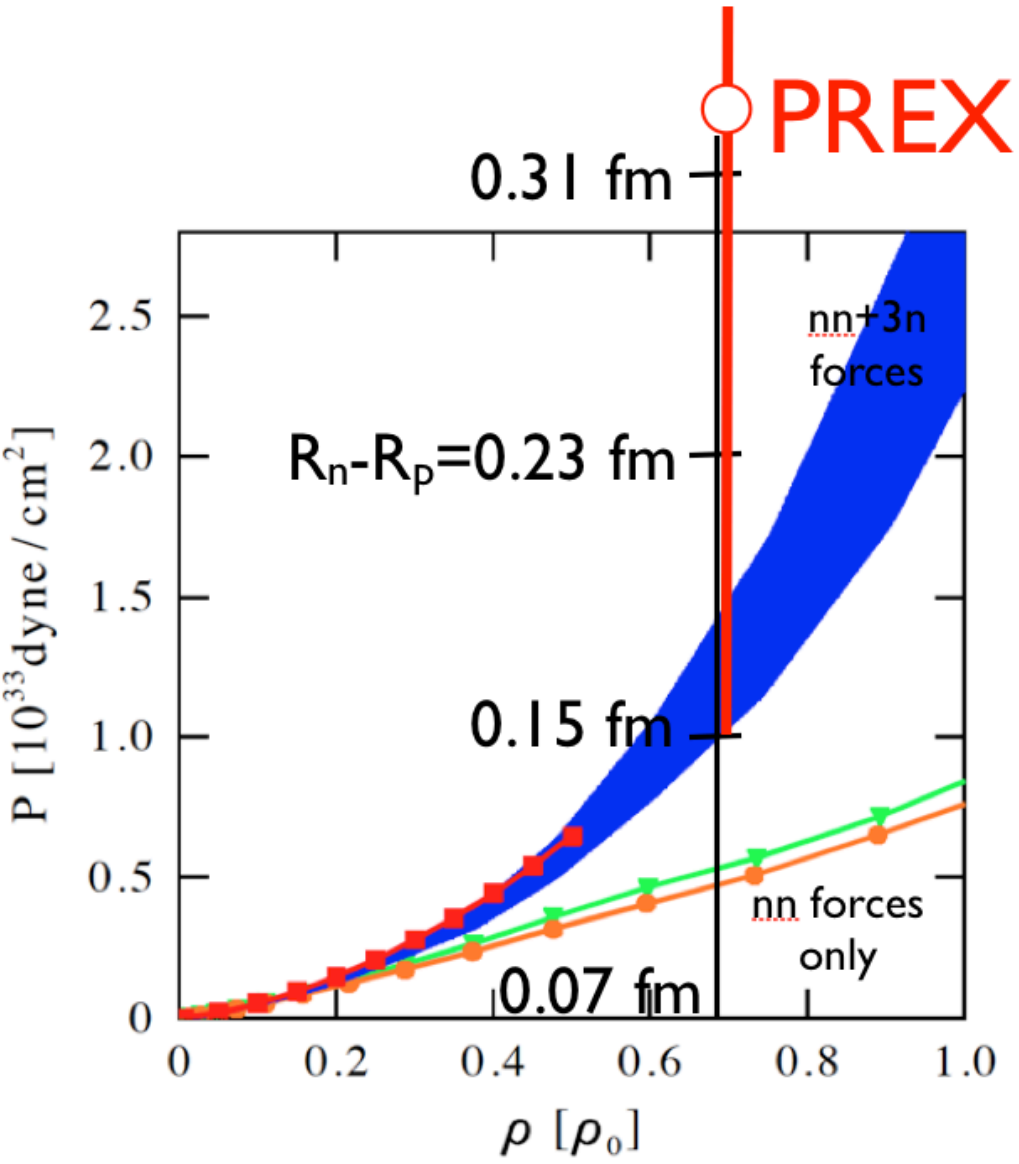


**FIGURE 1.** Pressure of neutron matter $P$ versus density, in units of nuclear density $\rho_0$, for chiral effective field theory calculations of Hebeler et al. including three neutron forces (blue band) or only with two neutron forces (green and brown lines). Also shown is the PREX result, Eq. 6, assuming Brown's correlation between skin thickness and $P$.

matter), demonstrated in Fig. 1.

In general the larger the pressure of neutron matter predicted by a given interaction, the further neutrons are pushed out against surface tension, and the larger the $R_n$. Therefore one expects some correlation between $R_n^{208}$ and $R_n^{48}$. In Fig. 2 we plot $R_n^{48} - R_p^{48}$ versus $R_n^{208} - R_p^{208}$ as predicted by a large number of relativistic and non-relativistic energy functionals [28]. One sees that there is some correlation where, in general, a large skin in Pb is correlated with a large skin in Ca. Furthermore there is about the same spread in skin thicknesses, $R_n^{208} - R_p^{208}$ varies from about 0.12 to 0.28 fm while $R_n^{48} - R_p^{48}$ varies from 0.14 to 0.24 fm. This suggests that 1% on $R_n^{48}$ is approximately as sensitive to nuclear structure effects as 1% on $R_n^{208}$. Three-neutron forces appear to change $R_n^{208}$ by about 0.05 fm, according to Hebeler et al, but in an indirect way. By taking this to set the scale of the effect, we conclude, that one should measure $R_n^{48}$ to at least an accuracy of 0.03 fm, in order to help constrain three-neutron forces and significantly impact nuclear structure. This proposal aims to measure $R_n^{48}$ to 0.03 fm.

There is some scatter in Fig. 2, see for example the black triangles which are calculated using a variety of non-relativistic Skyrme forces. This shows that there is additional nuclear structure information in measuring both $R_n^{48}$ and $R_n^{208}$ that is not contained in measuring just $R_n^{208}$ alone. For example electromagnetic spin-orbit currents make a larger contribution to $R_{ch}$ for $^{48}$Ca than for $^{208}$Pb [29]. Calculations are underway of the effect of weak spin orbit currents on the weak radius of $^{48}$Ca, and while this is believed to be a small effect that can be determined with small uncertainty such calculations, like those of the three-neutron forces, are rooted in present nuclear models.

A measurement of $R_n^{48}$ will test the $A$ dependence of the description of the neutron distribution, challenging the assumptions of nuclear models in extrapolating effects such as spin-orbit currents and three-neutron forces over a large lever-arm of size, charge, and mass number. Nuclear theory, in particular energy density functionals, can be accurately calibrated to reproduce both the measured $R_n^{208}$ in the relatively large nucleus $^{208}$Pb and $R_n^{48}$ in the much smaller $^{48}$Ca. This should allow much better extrapolations to predict $R_n$ in many other nuclei.

One important application of this is for the interpretation of atomic parity experiments. Atomic parity-violation (APV) is sensitive to the overlap of atomic electrons with the weak charge density of the nucleus and as a result, APV depends on $R_n$ [12,30,31]. A future low-energy test of the standard model may involve the combination of a precise APV experiment along with PV electron scattering to constrain $R_n$ [30]. There are ongoing APV experiments on Fr, Yb, and $Ra^+$ ions. In addition, APV is being measured for a range of Yb isotopes to provide information on neutron densities [32]. None of these nuclei are good candidates to directly measure $R_n$ via parity-violating electron scattering. Therefore it will be necessary to use theory to obtain $R_n$ in the

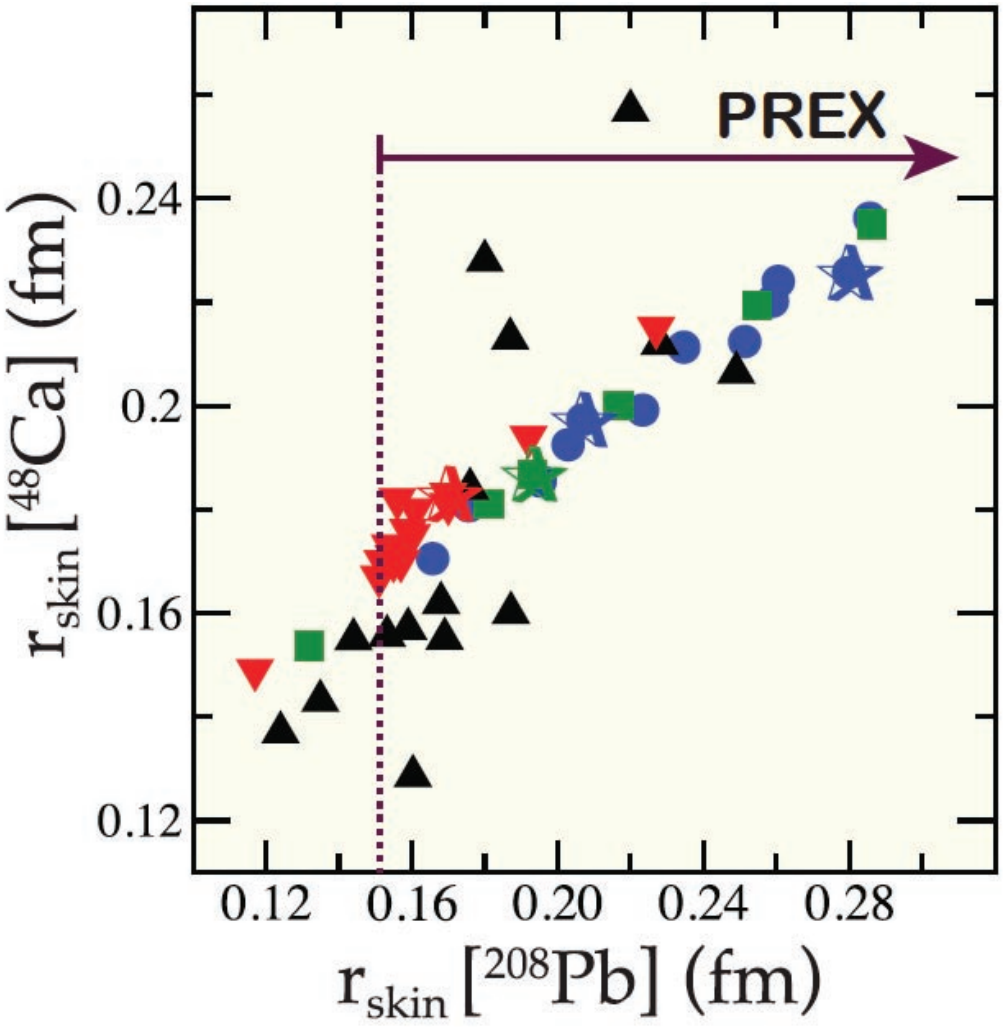


**FIGURE 2.** Thickness of neutron skin in $^{48}$Ca versus that for $^{208}$Pb for 48 relativistic and non-relativistic models (symbols) from [28]. Also shown is the PREX result for $^{208}$Pb.

APV system, and this theory can be accurately calibrated with measurements of both $R_n^{208}$ and $R_n^{48}$.

In summary, it is seen that the measurement of the $A_{PV}$ in $^{48}$Ca will serve as an important complement to the a measurement in $^{208}$Pb. Together they results test the predictions of state-of-the-art nuclear models by offering a range in $A$, where microscopic calculations can be applied to where the nucleus is closer to infinite neutron-rich nuclear matter. Applying the predictions from microscopic models, which cannot yet be done for $^{208}$Pb, could demonstrate the importance of three-neutron forces. Additionally, using the empirical correlations shown in models, $^{48}$Ca would reinforce the precision of the PREX measurement on $^{208}$Pb, which has a host of implications in nuclear and astrophysics.

## E Transverse Asymmetry Measurements

Parity-conserving single-spin asymmetry measurements with an unpolarized target can also be made if the beam polarization is set normal to the electron scattering plane ($A_T$). Such measurements are often used to control possible systematic errors in the longitudinal single-spin asymmetry $A_{PV}$, but recent results indicate a distinct physics motivation for the measurement of $A_T$. For this configuration, the asymmetry follows an azimuthal modulation

$$A_T = A_n \vec{P} \cdot \hat{k} \tag{7}$$

where $A_T$ is the transverse asymmetry, $A_n$ is the amplitude of the asymmetry modulation, $P$ is the polarization vector of the electron, and $\hat{k}$ is the unit vector of the cross product between the incoming and outgoing electron momentum vectors. This asymmetry is, in particular, a direct probe to multiple-photon exchange as it is vanishes in the Born-approximation by time reversal symmetry. The importance of understanding two-photon exchange, for example, has been highlighted by the discrepancy between $G_E^p$ measurements using Rosenbluth-separation and polarization observables [33].

Theoretical predictions are challenging to calculate due to the contributions from hadronic intermediate states in $\gamma - \gamma$ box diagrams and Coulomb distortion effects which are present for large $Z$. However, predictions have been made that these are on the order of a few ppm with beam energies of 1-2 GeV and $\theta_e \sim$ few degrees using the optical theorem with photoabsorption data [34] to describe the intermediate states. Different approaches, such as using generalized parton distributions to describe $e - p$ data [35], have also been taken.

Data for these asymmetries with $^1$H, $^4$He, $^{12}$C, and $^{208}$Pb are in preparation for publication at the time of this proposal by the HAPPEX and PREX collaborations and are shown in Fig. 3. There is significant disagreement from theory, particularly in $^{12}$C and $^{208}$Pb. The $^{208}$Pb measurement was most

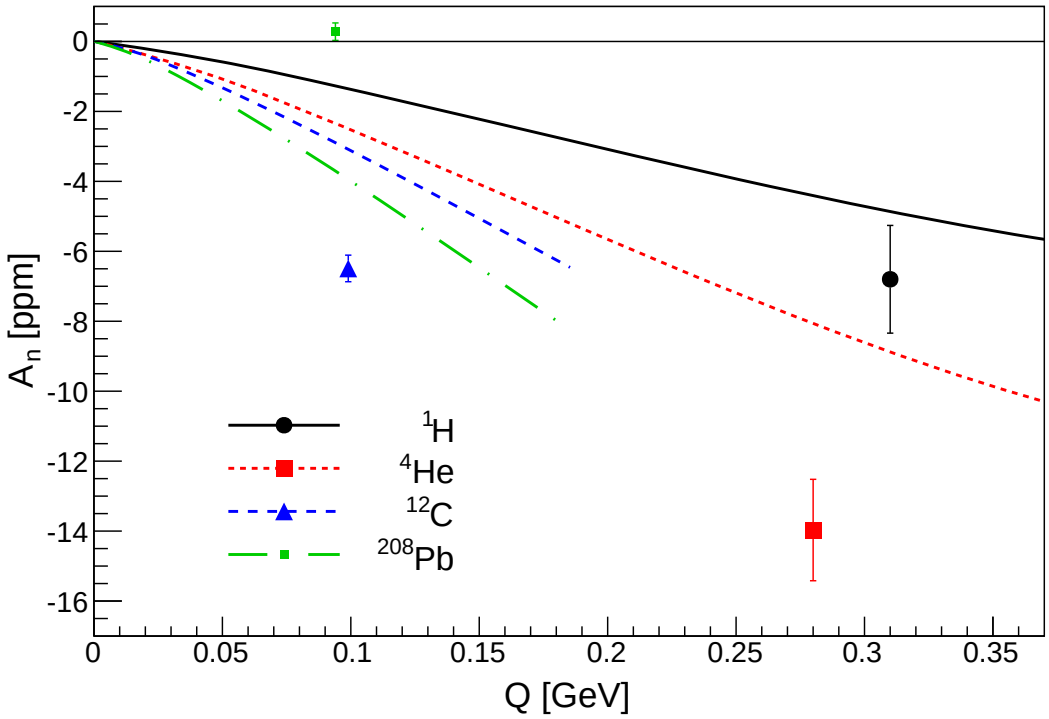


**FIGURE 3.** Extracted asymmetries $A_n$ vs. $Q$ for several different nuclei. The curves for each nucleus from [34] are also plotted.

surprisingly observed to be compatible with no asymmetry. The sources of disagreement are not presently well understood and investigations are underway, though Coulomb distortions and dispersion corrections are suspected to possibly contribute.

Measurements on $^{48}$Ca could be useful to help elucidate the dependence of these asymmetries on $Z$ and $Q^2$ by providing an additional data point. Because this asymmetry is so small, directly measuring it requires PV-type precision for which this experiment is designed. A precision of $\sim 0.5$ ppm would be on similar grounds as the previous data and would require significantly less running time than the proposed parity-violating measurement.

**TABLE 1.** Comparison of the 2005 HAPPEX-II experiment, the planned PREX-II measurement, and the CREX measurement proposed here.

| | HAPPEX-II | PREX | CREX |
|---|---|---|---|
| Energy | 3.1 GeV | 1.0 GeV | 2.2 GeV |
| Angle | 5.7 degrees | 5 degrees | 4 degrees |
| $A_{PV}$ | 1.4 ppm | 0.6 ppm | 2 ppm |
| rate | 100 MHz | 1 GHz | 100 MHz |
| precision | 7% | 1% (proposed) | 1% |

# II EXPERIMENTAL SETUP

## A Overview

The methods used in this measurement have been successfully used in PREX [24] and HAPPEX [36]. The main new apparatus elements for this proposal are the $^{48}$Ca target and a new septum magnet. The rest of the apparatus is standard equipment. The experiment is designed for 100 $\mu$A pass (2.2 GeV) beam. Table 1 highlights the experimental configuration and goals of this proposal relative to recent parity-violation experiments in Hall A. Because of larger transverse asymmetries which are a potential systematic in this measurement, we cannot run this experiment if the beam is not fully longitudinally aligned, requiring full polarization to the hall.

Longitudinally polarized electrons scatter elastically from an isotopically pure $^{48}$Ca target into the HRS (high-resolution spectrometers) in Hall A. To reach a 4° scattering angle, septum magnets are placed upstream of the HRS. The scattered electrons are detected by a calorimeter placed in the focal plane of the HRS, positioned to isolate the elastic peak and discriminate against inelastic levels. The electrons are integrated over each helicity window ($R$ and $L$ helicity) and an asymmetry is formed $A = \frac{\sigma_R - \sigma_L}{\sigma_R + \sigma_L}$.

We also plan on doing a measurement where the beam is polarized vertically-transverse (i.e. perpendicular to the electron scattering plane) at the same kinematics. The value of the asymmetry is not well known as discussed in Section I E, but to achieve a statistical uncertainty of 0.4 ppm, will require about two shifts of running at 100 $\mu$A.

# B Septum Magnet

The septum magnet will be a warm septum magnet similar to what was successfully used during PREx. A higher current density will be required, because the beam energy is 2.2 GeV (compared to 1.05 GeV) and because the scattered electron angle will be 4°. The two main issues when designing the septum are the hardware resolution and the acceptance. One needs sufficient hardware resolution to select the elastic peak with an integrating detector while discriminating the inelastic levels (the lowest level is 3.8 MeV for $^{48}$Ca). In order to achieve a 4° angle, the scattering chamber will need to be moved back $\sim$ 45 cm, which will reduce the solid angle. To achieve a good hardware resolution one needs a pure dipole magnetic field with negligible higher-order multipoles. The solid angle should be as large as possible, given the constraints on scattering angle and hardware resolution. Figure 4 shows the hardware resolution effects for the first few inelastic states (red) compared to the elastic peak $\delta = 0$ (black).

Because of damage to the old coils, new (identical) coils will have to be constructed for PREx II and APEx. CREx plans to use the two-coil configuration which was designed to improve the optics for PREx II (See Fig. 5), but with a higher current density ($\sim$1350 A/cm$^2$) in order to achieve the necessary field integral.

While this is an aggressively large current density, we note that it is smaller than that proposed for the MOLLER spectrometer coils, which has been subjected to an internal review by magnet experts. We plan to apply the lessons from those studies in designing new coils for this proposal.

The main concern is the size of the water-cooling hole; it needs to be large enough to avoid developing blockages due to erosion by the high flow velocity of the water. The current septum coils have a water-cooling hole twice as big as the smallest recommended hole size, so new coils with the same conductor will be adequate. A new power supply to drive the higher current, as well as additional LCW pumps (to achieve the necessary water flow to cool the coils) will be necessary.

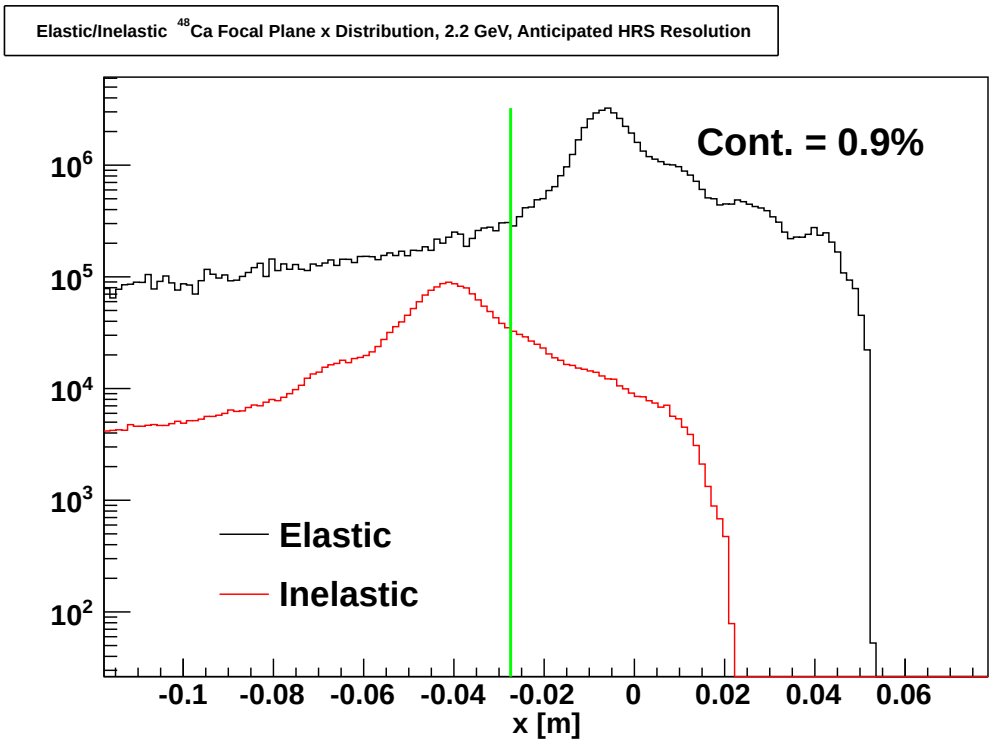


**FIGURE 4.** Elastic and inelastic spectrum after radiative and hardware resolution effects are folded in. The inelastic contributions to the measured sample, which are pushed into the elastic region, are about 1% of the events above the cut (green line).

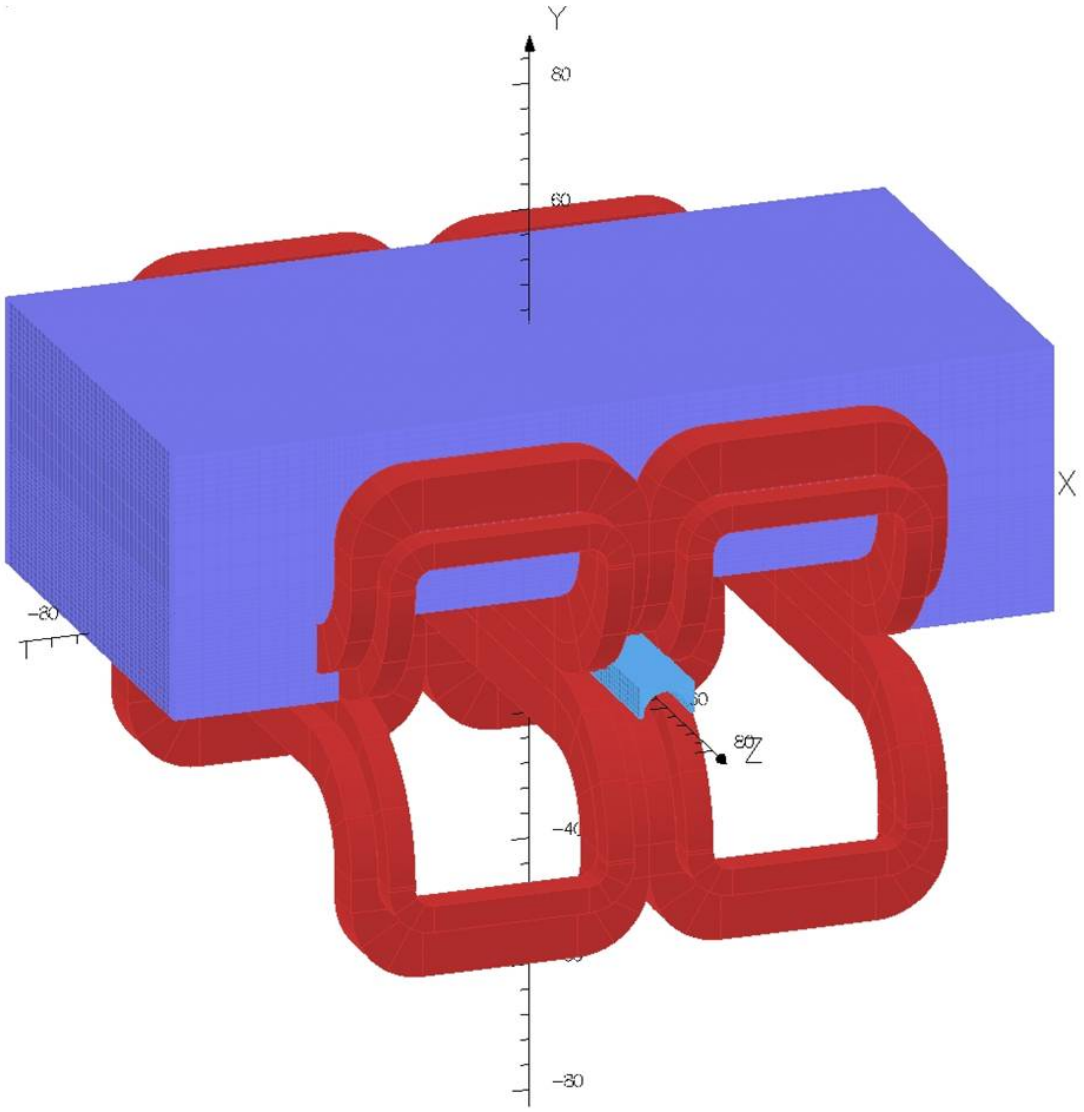


**FIGURE 5.** TOSCA picture of the two coil septum.

# C Calcium Target

The calcium target will be a 1 gm/cm$^2$ isotopically pure $^{48}$Ca target. Such a target was deployed in Hall A in the Spring of 2011 for the E08014 experiment, where it ran for several days of beam at 40$\mu$A. We are proposing to run at 2.5 times this current, i.e. 100$\mu$A. Thermal calculations show that with a standard raster pattern to distribute the heat from the beam, the target temperature will not exceed 120°C (the melting point is 842°C) if we can keep the temperature on the border of the target fixed at room temperature.

The target design concept is shown in Fig. 6. The $^{48}$Ca slab is housed in a vacuum chamber (probably stainless steel) with thin entrance and exit ("end-cap") windows. The chamber traps the atoms in case the target is destroyed, which is important since $^{48}$Ca is extremely expensive but can be recovered if the atoms are trapped in this chamber. This target design is similar to the one used during the E08014 experiment (see Figs. 7 and 8) except that this proposal calls for a longer target housing to allow electrons from 4° to clear the blocks located at the front and exit thin windows. The $^{48}$Ca slab can be recast to another thickness by Oak Ridge, provided it is a simple shape like a disk. The blocks are ∼1 cm thick, 25 cm long cylinders and therefore not much weight. The blocks serve two purposes: (a) to energy-degrade electrons that scatter from the end-cap windows so they don't reach our detectors, since they would cause background; and (b) the cryogenic cooling running through the blocks will carry away the 360 Watts of beam heating, thus cooling the $^{48}$Ca slab as well as the entrance and exit windows.

The end-cap windows need to be thick enough to withstand 1 atm pressure differential, while thin enough to not cause a large source of background. A thickness of ∼0.3 mm seems to be a practical compromise. The beam pipe should be no less than 3/4 inch diameter (1.9 cm) to accommodate beam delivery. In order to clear $4 \pm 1.3$ degrees using a standard $4 \times 4$ mm raster, the downstream block can be tapered, starting at a thickness of 2 mm nearest the target and increasing to 9 mm thick 15 cm further downstream. This will block electrons from the exit window that would have been in the acceptance. Electrons that scatter from the end-caps and pass through the block will lose typically $\geq$ 20 MeV by ionization loss through the material, and hence will not hit the detectors.

The thermal calculations assumed that the edge of the $^{48}$Ca slab is held at room temperature; this might not be the case; however, there is a lot of headroom on these calculations. What's more, we may do brief beam tests with an ordinary (inexpensive) calcium target during an earlier experiment such as PREX-II to see if the target can take 100 $\mu$A.

# D Detectors

The detectors will be similar to those used in PREX, where quartz will be used to detect Cerenkov photons. These will be connected to PMTs and the signal will be integrated in an existing data acquisition system previously used in other parity experiments and designed for its high linearity.

To minimize the size of the detectors which improves the light collection, a special optics tune for the spectrometers will be used which focuses the elastically scattered electrons into an area of several square centimeters. This area is above the vertical drift chambers by about a meter and the detectors will be mounted on a remotely controllable movable stand. This allows us to optimize the placement of the detectors with beam on target.

The collaboration has the experience of building these detectors from PREX. The design can be directly translated to this one by increasing the length of quartz to 13 cm based on optics simulations.

# E Kinematics Choice

The optimum kinematics of the experiment is the point which effectively minimizes the error in the neutron radius $R_n$. This is equivalent to maximizing the following product, which is the figure-of-merit (FOM) for this technique of neutron-density measurement: FOM $= R \times A^2 \times \epsilon^2$, where $R$ is the scattering rate, $A$ is the asymmetry, and $\epsilon = \frac{dA/A}{dR_n/R_n}$ is the the sensitivity of the asymmetry for a small change in $R_n$. Here, $dR_n/R_n$ is a fractional change in $R_n$ and $dA/A$ is a fractional change in $A$.

Using the high-resolution spectrometers (HRS) of Hall A, a small scattering angle maximizes the FOM. Given practical constraints on how low an angle ($4^\circ$) we can reach with septum magnets, the energy is fixed and turns out to be 2.2 GeV, which is a natural 1-pass beam energy for CEBAF operations in the 12 GeV era.

To evaluate the FOM a simple Monte Carlo was developed to calculate the rates for a given acceptance. The differential cross section, the asymmetry, and the sensitivity of the asymmetry on the neutron radius for $^{48}$Ca was supplied by C. J. Horowitz [37] which was calculated by numerically solving the Dirac equation and therefore includes Coulomb distortion effects.

Radiative losses were included by following the prescription by Mo and Tsai for nuclei [38]. A momentum acceptance cutoff of 3 MeV was used and amounted to about a factor of 2 reduction in accepted rate. Multiple scattering effects can distort the effective acceptance especially at small angles and are included by fully producing the Molière distribution. This was validated for several nuclei by comparing to a separate Geant4 simulation.

The acceptance for the spectrometers was taken to be based on the acceptance function as was measured during the PREX experiment, but shifted to

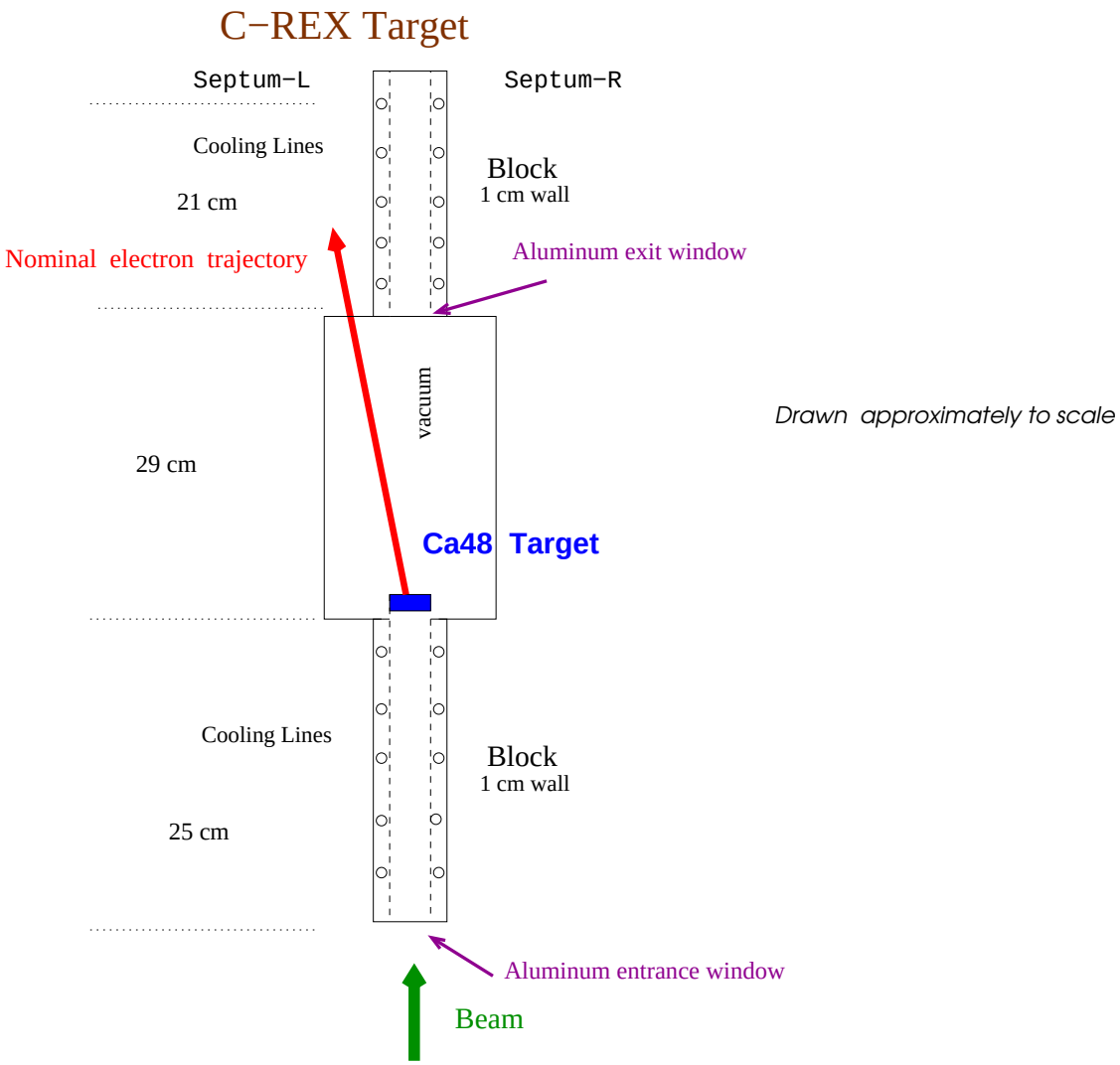


**FIGURE 6.** Conceptual drawing of the proposed $^{48}$Ca target design. A 1 gm/cm$^2$ thick isotopically pure $^{48}$Ca target is housed in a vacuum chamber. The chamber traps the atoms in case the target is destroyed. This is similar to the target used during the E08014 experiment (see Figs. 7 and 8) except that the design here calls for a longer target housing, with blockages on the entrance and exit windows to energy-degrade electrons that scatter from those windows, and with cryogenic cooling applied to the blocks, as shown, to carry away the 360 Watts of heat from the beam.

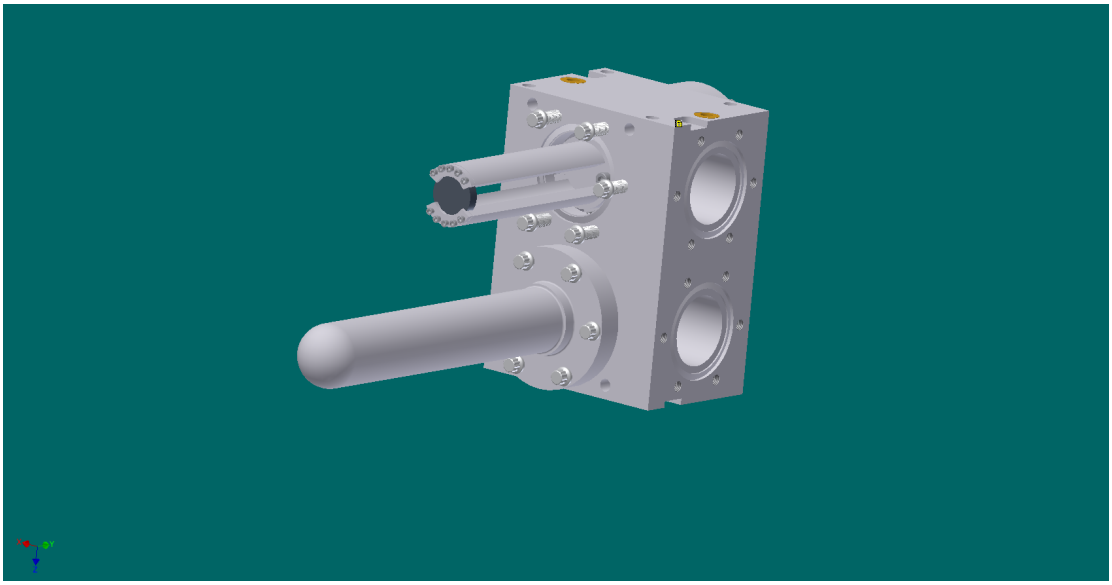

**FIGURE 7.** 3D view of the existing calcium target that has been used in Hall A during experiment E08014. For that experiment, two targets were mounted on one block. The picture shows one target with the inner part exposed. The two targets used were $^{40}$Ca and $^{48}$Ca. For C-REX, this target will be modified significantly, see fig 6 for the target of this proposal. It will be longer and there will be blockages on the entrance and exit windows to energy-degrade electrons from them so they don't reach the detector.

4° and including solid angle scaling due to the target being further away by 0.45 m and being moved to smaller angle. The overall solid angle subtended by each spectrometer by this technique was about 1.6 msr. This represents a conservative estimate of what can be achieved.

For running conditions, a beam current of 100 $\mu$A with energy 2.2 GeV and 85% polarization and a 5% radiation length (1 g/cm$^3$) target was assumed. A running time of 30 days was used with no considerations for downtime. In Figs. 9, 10, and 11 the rate, measured asymmetry, and asymmetry sensitivity to the neutron radius, $\epsilon$ is plotted. The error in the neutron radius, Fig. 12, is minimized where the FOM is maximized. A 1.8% assumed systematic error changes the optimum FOM kinematics, as noted in the figure.

## F Polarimetry

The Compton and Møller polarimeters in Hall A should achieve a 1% accuracy in beam polarization during the run. Improvements in polarimetry will continue during the approved PREX-II experiment and are of vital importance to the entire future Hall A program. Because of the higher energy, the Compton polarimeter will have a higher figure-of-merit and lower systematic errors than during PREX-I.

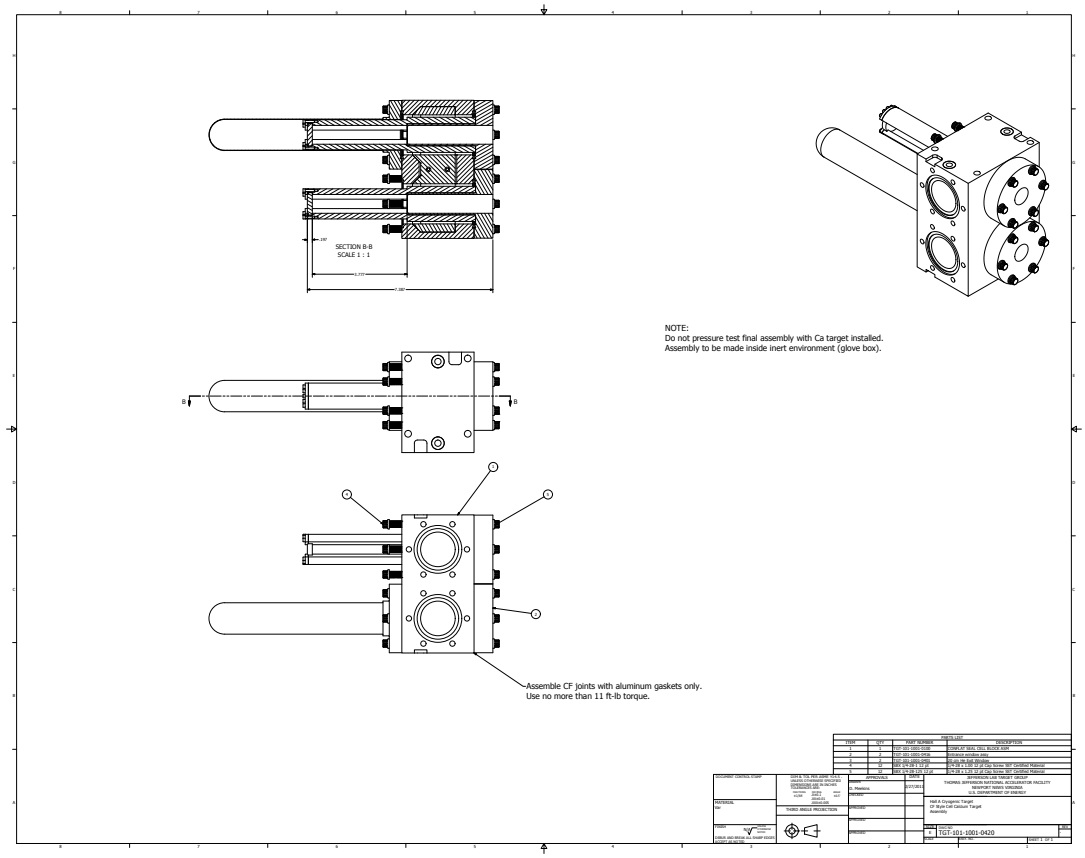


**FIGURE 8.** Engineering drawings of the existing $^{48}$Ca target used during E08014. See the figure caption for Fig. 7.

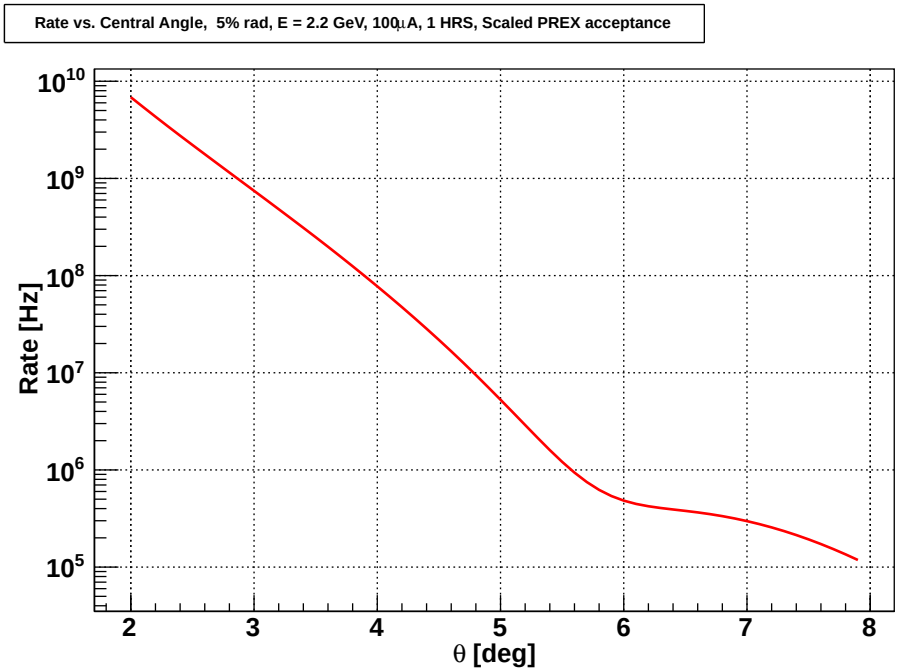


**FIGURE 9.** Rates for 1 HRS versus angle for 2.2 GeV; this calculation was done at 100$\mu$A.

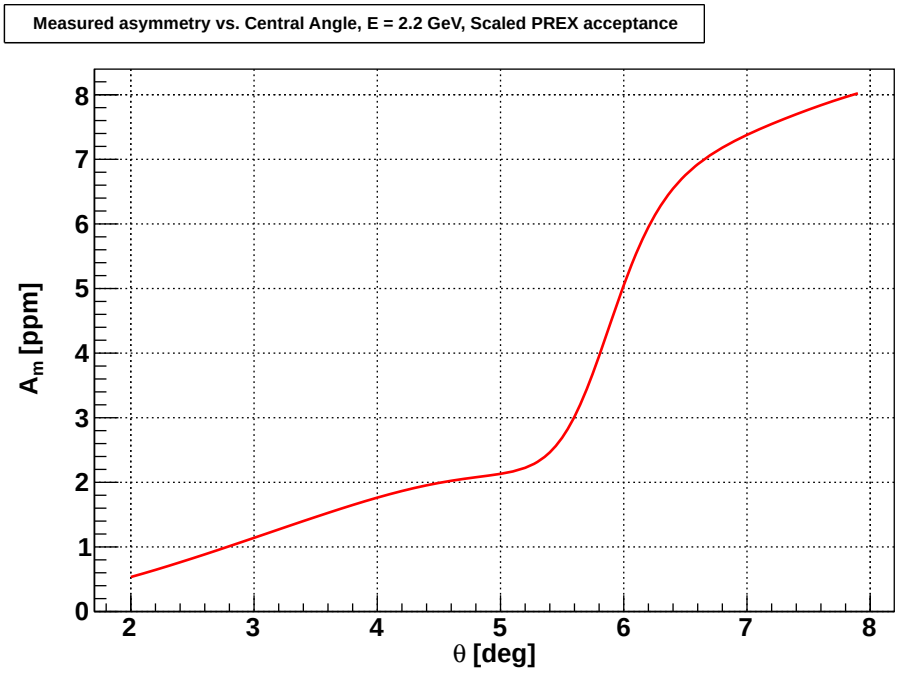


**FIGURE 10.** Measured asymmetries versus angle for 2.2 GeV. A factor of 0.85 for the beam polarization is included.

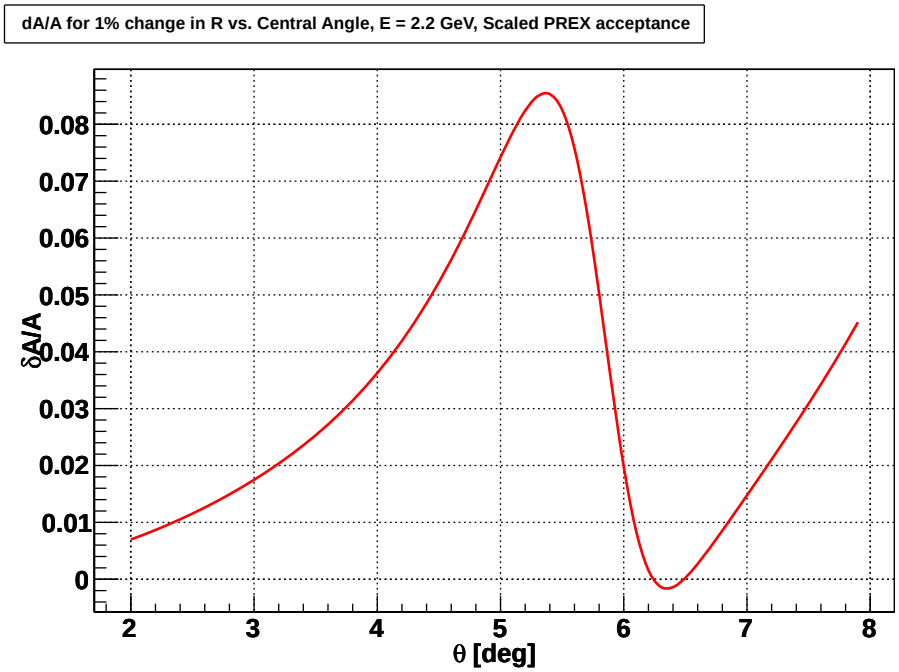


**FIGURE 11.** Sensitivity of the asymmetry to a 1% change in $R_n$ versus angle for 2.2 GeV.

## *1 Møller Polarimeter*

In 2009 - 2010, the Møller polarimeter was upgraded as follows: 1) The "brute force" polarization of the target foil using a strong (3T) magnetic field, as has been done in Hall C [39]. Also the target has a smaller thickness and lower heating; 2) A segmented aperture detector to accommodate the higher rates; and 3) A new fast DAQ based on Flash ADCs to handle the higher rates with smaller deadtime and to provide more information about the events such as pileup. Table 2 shows the systematic errors achieved during PREX-I which totaled 1.1%. Incremental improvements in the systematic error are expected.

## *2 Compton Polarimeter*

The Compton polarimeter was upgraded in 2009 - 2010 to achieve an improved figure of merit at low energies by using a new green laser and a new resonant cavity and refurbished optics table. The signals from back-scattered photons were integrated in custom Flash ADCs. This integration technique eliminated the systematic error from thresholds that affected the older counting method. Table 3 shows the systematic errors achieved during PREX-I which totaled 1.2%, a major accomplishment for 1 GeV running. At the 2.2 GeV beam energy of this proposal, the Compton Polarimeter will operate with

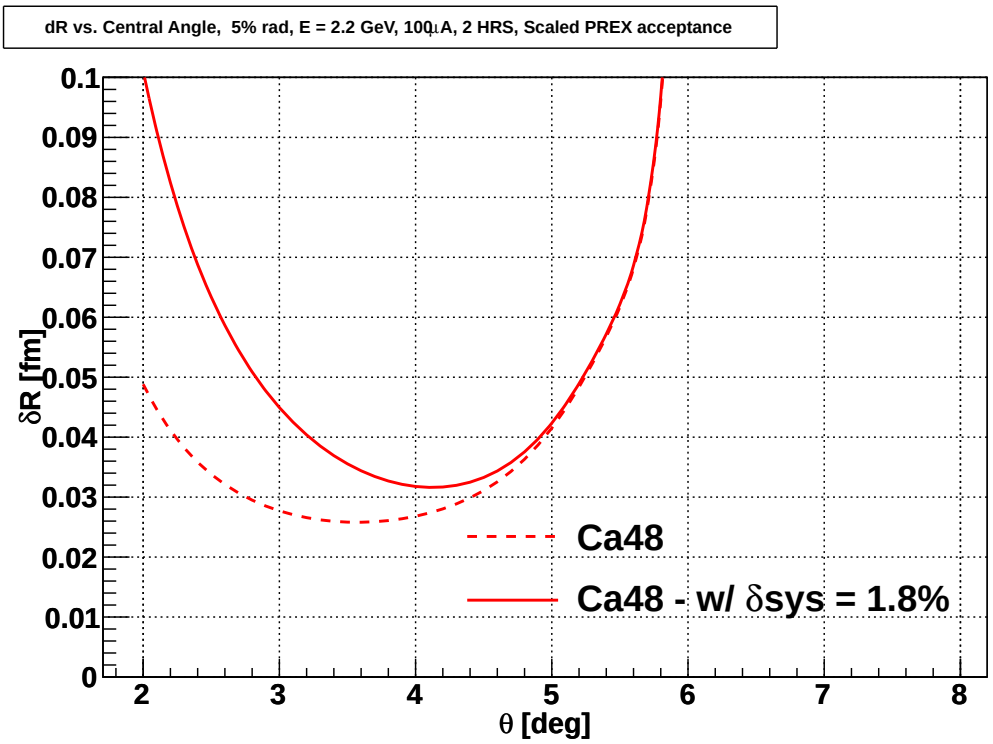


**FIGURE 12.** Error in $R_n$ versus angle for 2.2 GeV (1-pass beam) for 30 days at 100$\mu$A for a target thickness of 5% radiation length. An error of 0.03 fm is feasible. With a 1.8% assumed systematic error (solid curve), the optimal angle is 4°. The dashed curve shows the statistical error only. At this angle the total error is close to being minimized. Note that apart from the fact that smaller angles are not feasible, the smaller angle would also increase the rates and reduce the asymmetries, which would increase the relative systematic errors.

**TABLE 2.** Møller Polarimeter Systematic Errors

| | |
|---|---|
| Iron Foil Polarization | 0.25% |
| Targets Discrepancy | 0.5% |
| Target Saturation | 0.3% |
| Analyzing Power | 0.3% |
| Levchuk Effect | 0.5% |
| Target Temperature | 0.02% |
| Deadtime | 0.3% |
| Background | 0.3% |
| Other | 0.5% |
| Total | 1.1% |

**TABLE 3.** Compton Polarimeter Systematic Errors

| | |
|---|---|
| Laser Polarization | 0.7% |
| Gain Shift | 0.9% |
| Collimator Position | 0.02% |
| Nonlinearity | 0.3% |
| Total | 1.2% |

**TABLE 4.** Systematic Error Contributions in C-REX

| | |
|---|---|
| Charge Normalization | 0.1% |
| Beam Asymmetries | 0.3% |
| Detector Non-linearity | 1.0% |
| Transverse | 0.1% |
| Polarization | 1.2% |
| Inelastic Contribution | 0.5% |
| $Q^2$ | 0.8% |
| Total | 1.8% |

higher figure-of-merit and lower systematic errors than at 1 GeV. Therefore we can expect to have 1% accuracy from Compton.

## G Systematic Errors

The total systematic error goal is about 1.8% on the asymmetry, compared to an anticipated statistical accuracy of 2.8%. The dominant contributions are all from effects which have been well understood in previous experiments [24,36].

### *1 Beam Induced Asymmetries*

At the end of 6-GeV era parity running, PREX was able to achieve overall asymmetry corrections due to helicity-correlated beam position fluctuations of about 40 ppb with position differences $< 4$ nm. The position/asymmetry correlations are regressed out of the measured asymmetry using two independent methods: first, directly observing the asymmetry correlations by the natural beam motion and second, by systematically perturbing the beam through a set of magnetic coils (dithering). Achieving these small values was possible in part by periodically inserting the half-wave plate and the injector and flipping the helicity of the beam using a double-Wien filter which helps them cancel over time.

The correction made was dominated by fluctuations in the beam intensity due to small changes in the accepted angle and the sharply falling lead cross

section. As we are at higher $Q^2$ ($0.022$ $(\mathrm{GeV/c})^2$) and $^{48}$Ca is a smaller nucleus, $d\sigma/d\theta$ is smaller by a factor of six. We will conservatively assume that the uncertainty on the corrections we apply will be 7 ppb, the same as PREX-I.

The integrated signals in the helicity windows are normalized to the beam current monitor signals to remove helicity correlated beam intensity fluctuations. Non-linearities in the BCMs produce additional false asymmetries, which are related to the overall charge asymmetry. Based on past running, we can expect an cumulated charge asymmetry less than 100 ppb and an uncertainty on that correction of 1.5%, so 1.5 ppb, or 0.1% propagated to the final asymmetry.

## *2 Inelastic Contributions*

The first few inelastic excited states were simulated with the appropriate strengths by using fits to form factor measurements of electron scattering from $^{48}$Ca done at MIT-Bates [40]. These measurements covered the same momentum transfer range of interest here.

Elastic and inelastic states were simulated with a radiative tail and the resolution presented in Fig. 4. Of particular importance is the fact that the resolution tends to push lower energy particles into higher momentum bins, increasing the relative number of inelastics. They contribute about 1% to the total accepted events. This is a baseline and improvement in the hardware optics resolution will reduce this amount.

Calculation of the contributing asymmetries is underway, but they are not expected to be significantly different from the measured asymmetry. Assuming this, and assuming calculations are reliable to within 50%, this corresponds to a 0.5% systematic uncertainty from the contamination.

## *3 $Q^2$ Measurement*

For the kinematics of the experiment, the change of the asymmetry with respect to the electron scattering angle is sufficient such that our ability to measure the angle contributes to an effective uncertainty in the asymmetry. For $^{48}$Ca at 4° with 2.2 GeV beam, $dA/dQ^2 \sim -60$ ppm/GeV$^2$, or $-40$ ppm/rad.

To measure the scattering angle, survey techniques will be insufficient to constrain the propagated uncertainty to less than 1%. By utilizing a proton target and comparing the energy difference between the elastically scattered electron peak and the elastic peak from a heavier nucleus, the absolute angle can be fixed. Such a technique was used for PREX and obtained an angle resolution of about 0.4 msr. Given comparable energy resolution (after optics calibration), and taking into account the kinematic differences, a similar angular resolution can be achieved for this experiment. This corresponds to an 0.8% uncertainty in the measured asymmetry.

Additionally, the relative acceptance of the spectrometers must be measured so the asymmetry, integrated over the acceptance, can be related to an effective $Q^2$. Periodically through the experiment dedicated $Q^2$ runs will be taken at a low beam current ( $\sim 100$ nA) which allows for the vertical drift chambers to be operated and provide high resolution event-based tracking.

## *4 Transverse Asymmetry*

If the beam has a transverse component of polarization, a parity-conserving asymmetry is introduced into the spectrometers with an azimuthal modulation. By running both spectrometers symmetrically and summing over the signals, this component will largely cancel. However, the parity-conserving value is typically larger than the parity-violating and may be a potential contamination if the spectrometers are place asymmetrically.

The value of the transverse asymmetry from $^{48}$Ca is presently poorly constrained by theory (as discussed in Section I E), but has been measured at similar $Q^2$ points for several nuclei, Fig. 3. A realistic estimate is that it will be about 8 ppm, or about 4 times larger than the proposed measured asymmetry.

To control this potential systematic, we plan to measure this asymmetry directly during the experiment to a statistical precision of 0.4 ppm and place collimators which are aligned to symmetrize the acceptance. If the collimators are placed vertically within 1 mm of the ideal positioning, the asymmetry is suppressed by a factor of 100. If the beam polarization is longitudinally oriented to within 1° then the transverse asymmetry is suppressed by another factor of 50. Because the asymmetry is only a factor of 4 larger, the overall change in the asymmetry is suppressed to about $10^{-3}$, and therefore a very small effect.

# III RADIATION IN THE HALL

It is well-known that PREX-I suffered from radiation damage of equipment in Hall A which caused down-time for the experiment to repair electronics, as well as damage to soft O-rings that were used in the vacuum system downstream of the target. These problems and their mitigation are described in the PREX-II proposal [41]. In particular, we plan to make improvements to the radiation-shielding and to use hard metal seals for the vacuum chambers. For the present proposal, we have computed with Geant4 the power from neutrons, photons, and electrons from the target and collimator. The most damaging component during PREX-I was the neutrons. In order to mitigate this, the collimator bore will be reduced to isolate the source of neutrons, and then it will be shielded. For $^{48}$Ca the power from neutrons per incident electron from the collimator region is a factor of 10 less than for PREX-II (see Fig. 13), so although the shielding configuration will have to be optimized for CREx, it will be possible to reduce the neutron backgrounds significantly below the PREx-I levels.

Note, PREX-II will run at 70$\mu$A, i.e. 70% of this proposal. The power from photons per incident electron is also an order of magnitude smaller for this proposal, while the power from electrons is comparable. Therefore, we believe the strategies developed for PREX-II will be adequate for this proposal.

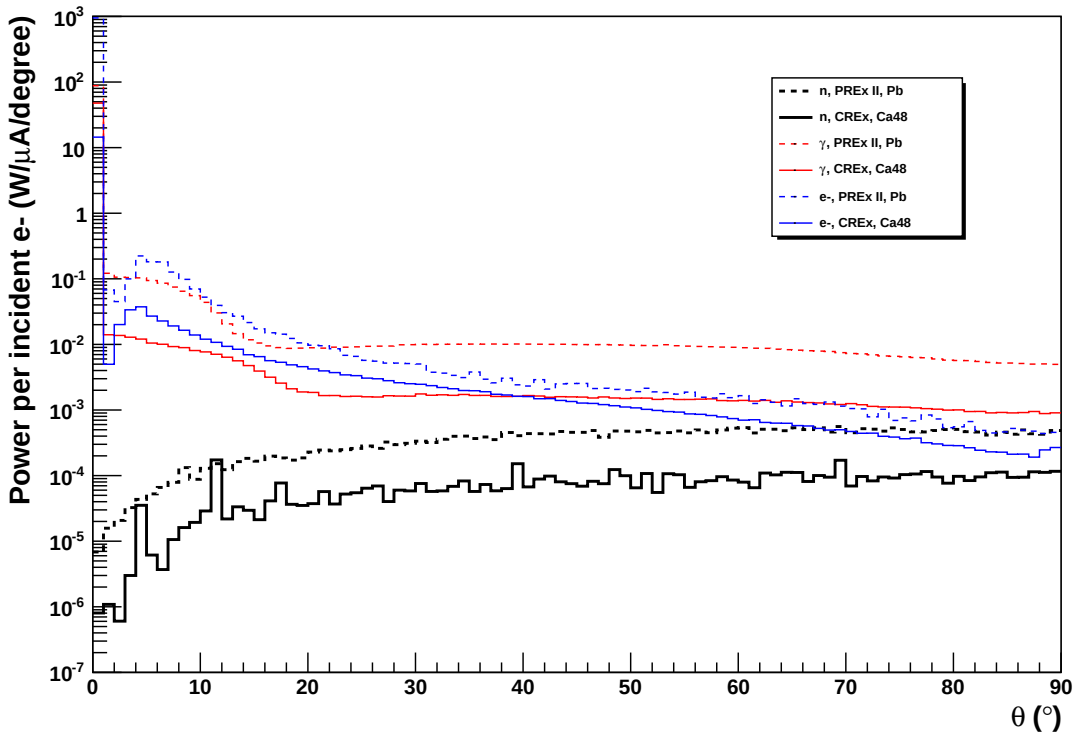


**FIGURE 13.** Plot of the power of particles from the target and collimator as a function of angle incident on a sphere centered on the target. The power from each type of particle - neutrons (black), photons (red) and electrons (blue) is compared between PREx II (dashed lines) and CREx (solid lines), with the appropriate target, collimator and energy. The dip in the electron and photon plots is because of the presence of the collimator; the entrance to the beam dump is $\sim 1^\circ$, so above this angle the power would be incident in the hall somewhere. Most of the neutrons originate in the collimator itself. The power from neutrons and photons (per $\mu$A) for CREx is about an order of magnitude smaller than PREx.

**TABLE 5.** C-REX Proposed Data

| | |
|---|---|
| Measured Asymmetry ($p_e$ $A$) | 2 ppm |
| Beam Energy | 2.2 GeV |
| Scattering Angle | 4° |
| Beam Current | 100$\mu$A |
| Statistical Uncertainty of $A_{PV}$ | 2.8% |
| Systematic Uncertainty of $A_{PV}$ | 1.8% |
| Statistical Uncertainty of $A_T$ | 0.4 ppm |
| Detected Rate (each spectrometer) | 80 MHz |
| C-REX Production | 30 days |
| Setup, Calibrations, Møller | 10 days |
| Total Time Request | 40 days |

# IV BEAM TIME REQUEST

We request 40 days of polarized beam running in Hall A at 2.2 GeV using a new 4° degree septum magnets. This includes 5 days of commissioning and 5 days of overhead for Møller Polarimetry, transverse asymmetry, and auxiliary measurements. See Table 5. All beam for CREX production must be fully longitudinally polarized. We will need 2 days of beam vertically polarized for the transverse measurement and systematic checks.

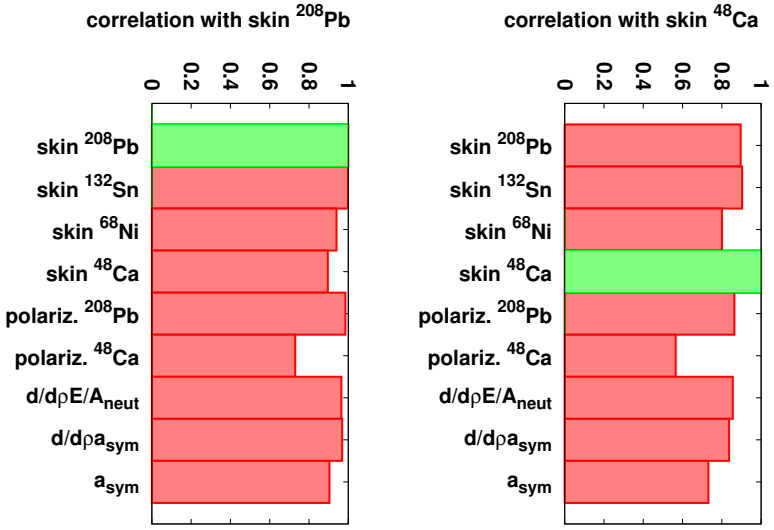


**FIGURE 14.** A catalog of correlations between the neutron skin thickness $R_n - R_p$ of $^{208}$Pb and $^{48}Ca$ and various parameters of nuclear structure models. Labels are described in the text. [42]

# A APPENDIX: CORRELATION OF $R_N$ WITH NUCLEAR STRUCTURE OBSERVABLES

Note: This section is excerpted from a report authored by P. G. Reinhard and collaborators [42].

Correlation between neutron skin $R_nR_p$ in $^{208}$Pb (left) or $^{48}$Ca (right) and a couple of other observables: "skin" the neutron skin, "polariz." the dipole polarizability, $d/d\rho E/A_{neut}$ the slope of the neutron EoS at $\rho = 0.08$ fm$^3$, $d/d\rho_{\rm asym}$ the slope of the symmetry energy at $\rho = 0.08$ fm$^3$, and asym the symmetry energy. These are the observables which correlate most strongly to the skins. All others stay below a correlation of 1/2. The trivial self-correlation is indicated by a green box.

The case of $^{208}$Pb (left panel) shows very strong correlations to the bulk asymmetry properties and to polarizability in $^{208}$Pb. There are also strong correlations to the neutron skin in other nuclei, however decreasing with increasing distance to $^{208}$Pb. The correlation to the polarizability in $^{48}$Ca is also significantly reduced. The case of $^{48}$Ca (right panel) shows also strong correlations to most of the observables under consideration. However, these correlations are generally reduced as compared to the case of $^{208}$Pb. Thus the information content of the skin in $^{48}$Ca with respect to collective properties is not as large as it was for $^{208}$Pb.

# REFERENCES


1. B. Frois et al., Phys. Rev. Lett. **38**, 152 (1977).
2. C. Garcia-Recio, J. Nieves and E. Oset, Nucl. Phys. A **547**, 473 (1992).
3. L. Ray, W. R. Coker, G. W. Hoffmann, Phys. Rev. C **18**, 2641 (1978).
4. V. E. Starodubsky, N. M. Hintz, Phys. Rev. C **49**, 2118 (1994).
5. B. C. Clark, L. J. Kerr, S. Hama, Phys. Rev. C **67**, 054605 (2003).
6. A. Trzcinska et al., Phys. Rev. Lett. **87** , 082501 (2001).
7. H. Lenske, Hyperfine Interact. **194**, 277 (2009).
8. A.M. Bernstein, W.A. Seidler, Phys. Lett. B **34**, 569 (1971) Physics Letters B, **34**, Issue 7, 1971, Pages 569-571
9. A.M. Bernstein, W.A. Seidler, Phys. Lett. B **39**, 583 (1972).
10. T. W. Donnelly, J. Dubach, Ingo Sick, Nucl. Phys. **A503**, 589 (1989).
11. C. J. Horowitz, Phys. Rev. C **57** , 3430 (1998).
12. C. J. Horowitz, S. J. Pollock, P. A. Souder, R. Michaels, Phys. Rev. C **63**, 025501 (2001).
13. B. A. Brown, Phys Rev. Lett. **85**, 5296 (2000).
14. C. J. Horowitz, J. Piekarewicz, Phys. Rev. **C64**, 062802 (2001).
15. F. Ozel, G. Baym, T. Guver, Phys. Rev. D **82**, 101301 (2010).
16. A. W. Steiner, J. M. Lattimer, E. F. Brown, Astrophys. J. **722**, 33 (2010).
17. W. G. Lynch, M. B. Tsang, Y. Zhang, P. Danielewicz, M. Famiano, Z. Li, A. W. Steiner ArXiv:0901.0412.
18. M.B.Tsang, Yingxun Zhang, P.Danielewicz, M.Famiano, Zhuxia Li, W.G.Lynch, A.W.Steiner, Phys. Rev. Lett. **102**, 122701 (2009).
19. C.J. Horowitz, J. Piekarewicz, Phys. Rev. **C66**, 055803 (2002).
20. C. J. Horowitz, J. Piekarewicz, Phys. Rev. Lett. **86**, 5647 (2001).
21. L. Baiotti, B. Giacomazzo and L. Rezzolla, delayed collapse to black hole," Phys. Rev. D **78**, 084033 (2008) [arXiv:0804.0594 [gr-qc]].
22. P. G. Reinhard, W. Nazarewicz, Phys. Rev. C **81**, 051303 (2010).
23. A. Tamii et al., Phys. Rev. Lett. **107**, 062502 (2011).
24. S. Abrahamyan *et al.*, Phys. Rev. Lett. 108, 112502 (2012).
25. C.J. Horowitz, *et al.*, Phys. Rev. C 032501 (2012).
26. K. Hebeler, J. M. Lattimer, C. J. Pethick, A. Schwenk, Phys. Rev. Lett. **105**, 161102 (2010).
27. G. Hagen, M. Hjorth-Jensen, G. R. Jansen, R. Machleidt, and T. Papenbrock, arXiv:1204.3612v1
28. J. Piekarewicz *et al.*, Phys. Rev. C **85**, 041302 (2012)
29. J. Piekarewicz, private communication.
30. S. J. Pollock, E. N. Fortson, and L. Wilets, Phys. Rev. C **46**, 2587 (1992); S.J. Pollock and M.C. Welliver, Phys. Lett. B **464**, 177 (1999)
31. B. A. Brown, A. Derevianko, V. V. Flambaum, Phys. Rev. C **79**, 035501 (2009).
32. K. Tsigutkin, D. Dounas-Frazer, A. Family, J. E. Stalnaker, V. V. Yashchuk, D. Budker, arXiv:1001.0587.
33. C.F. Perdrisat, V. Punjabi, M. Vanderhaeghen, Prog. Part. Nucl. Phys. **59**, 694 (2007).

34. M. Gorchtein, C.J. Horowitz, Phys. Rev. C **77**, 044606 (2008).
35. A.V. Afanasev, S.J. Brodsky, C.E. Carlson, Y.-C. Chen, M. Vanderhaeghen, Phys. Rev. D **72**, 013008 (2005).
36. K. A. Aniol *et al.*, Phys. Rev. Lett. **82** 1096 (1999). K. A. Aniol, *et al.*, Phys. Rev. C 69, 065501 (2004). K. A. Aniol, *et al.*, Phys.Rev.Lett.96:022003,2006. K. A. Aniol, *et al.*, Phys.Rev.Lett.98:032301,2007.
37. C.J. Horowitz, Phys. Rev. C **57**, 3430 (1998).
38. L.W. Mo and Y.S. Tsai, Rev. Mod. Phys. **41**, 205235 (1969).
39. M. Hauger *et al*, Nucl. Instr. and Methods A 462 (2001) 382.
40. Phys. Rev. C 31, 1699 (1985).
41. Jefferson Lab Experiment E12-11-101 (PREX-II). Proposal available at http://hallaweb.jlab.org/parity/prex
42. P. G. Reinhard *et al.*, Private Communication.